Inverted hysteresis loops in magnetically coupled bilayers with uniaxial competing anisotropies: Theory and experiments

S. M. Valvidares, L. M. Álvarez-Prado, J. I. Martín, and J. M. Alameda
Laboratorio de Magnetoóptica, Departamento de Física, Universidad de Oviedo c/ Calvo Sotelo, s/n, E-33007 Oviedo, Spain
(Received 5 October 2000; published 13 September 2001)

The magnetization reversal processes in magnetic bilayers with individual uniaxial anisotropies have been studied, both theoretically and experimentally, to analyze the possible existence of inverted hysteresis loops, that is, with negative remanent magnetization (M_r). Kerr effect measurements in amorphous YCo_2/YCo_2 bilayers and alternating gradient magnetometry in polycrystalline FeNi/FeNi samples reveal that $M_r<0$ can be observed for certain directions of the applied magnetic field in the sample plane. This property has also been found in CoNbZr films annealed under an applied field. Our theoretical approach shows that the behavior of these magnetic heterogeneous systems with two coupled uniaxial anisotropies can be understood in terms of two competing effective anisotropies, one biaxial (with K_{biax}) and one uniaxial (with K_{uniax}). In particular, a phase diagram has been deduced for the conditions on K_{biax} and K_{uniax} that can produce negative remanence. This description indicates that, under those anisotropy conditions, inverted hysteresis loops can be observed for an applied field close to the hard axis of the effective uniaxial anisotropy, when magnetization reversal is driven by rotations and not by domain nucleation and wall movement. To consider the real situation in a YCo_2/YCo_2 bilayer sample, the predictions of this phenomenological model have been further improved by micromagnetic calculations, which are in very good agreement with the magneto-optical measurements.

DOI: 10.1103/PhysRevB.64.134423 PACS number(s): 75.30.Gw, 75.70.−i, 75.60.Ej

I. INTRODUCTION

The study of magnetization processes in magnetically heterogeneous systems, where regions with different magnetic anisotropies are magnetically coupled, is nowadays a research field of great interest. Important examples of these systems are magnetic multilayers,[1] spin valves,[2] or nanostructured systems where two magnetic phases coexist.[3] Depending on the particular configuration of the magnetic coupling, a variety of magnetization behaviors can be present even in simple systems.

An important case, interesting from the fundamental and applied points of view, is the study of magnetic bilayers, where the presence of an intermediate nonmagnetic layer can produce an effective coupling between magnetizations of 0° (ferromagnetic), 180° (antiferromagnetic), or 90° (biquadratic), due to the oscillatory behavior of the bilinear indirect exchange as a function of the intermediate layer thickness.[4–8] Also, in magnetic bilayers without any kind of separating layers, effective couplings either of 0° or 180° can be found.[9,10] Several important factors must be considered to understand the properties of these systems; the symmetry, magnitude, and orientation of the anisotropy in each layer are fundamental to analyze the magnetization processes and the torque magnetometry measurements,[11,12] and, furthermore, the global magnetostatic coupling[13–15] and the coupling between domain walls[16–18] must be taken into account for the study of bilayers without exchange coupling.

In fact, the role played by anisotropies of the layers in the magnetization reversal has attracted a great interest; in this way, a theoretical study has been reported on the magnetization processes in antiferromagnetically coupled multilayers when cubic and uniaxial anisotropies are present.[11] Also, ferromagnetic coupling has been considered in equivalent systems to analyze magnetization equilibrium states at zero applied field.[19] Experimentally, systems of coupled bilayers with orthogonal uniaxial anisotropies have been considered, either in the case of two planar anisotropies[20] or when one of them is perpendicular to bilayer plane.[21]

One of the most suggestive behaviors of magnetically heterogeneous systems is the possible presence of inverted hysteresis loops, that is, with a negative remanence. These loops have been theoretically predicted for ultrathin films with competing uniaxial and biaxial anisotropies.[22] Also, they have been observed in several systems, but their particular interpretations are based on different origins; inverted loops are found in Co-O-based compounds,[23] where they are justified by the exchange anisotropy,[24] in Ag/Ni multilayers[25] and (Ni,Fe)-SiO_2 granular films,[26] interpreted by the magnetostatic interactions,[26,27] and in epitaxial Fe(111) films, where they have been related to the component of the magnetization that is perpendicular to film plane.[28] On the other hand, to our knowledge, the existence of inverted hysteresis loops in one of the most simple magnetic systems, such as a bilayer coupled by ferromagnetic direct exchange, has not been analyzed.

In this work, we report, experimentally and theoretically, the presence of inverted loops in magnetic bilayers where the two ferromagnetic coupled layers have individual uniaxial anisotropies in the sample plane. The general case of anisotropies with different magnitudes in each layer and different relative orientations has been considered. Our theoretical approach generalizes a model proposed by Torok *et al.*,[29] and it is found that the global behavior of the bilayer can be described as the competition of a biaxial and an uniaxial anisotropies acting on the average magnetization of the sample. Therefore, the magnetization processes can be analyzed in a similar framework to the model proposed by Arrot

for ultrathin films.[22] We have clarified the anisotropy conditions and the applied field directions that result in the observation of hysteresis loops with negative remanence in this simple systems, making a detailed comparison with the experimental results.

This article is organized as follows: In Sec. II we present the different samples used for this work together with the experimental characterization of the inverted hysteresis loops. Our theoretical study is included in Sec. III, where we have also performed micromagnetic numerical calculations to consider the width of the domain walls neglected in the analytical model. Finally, in Sec. IV we compare theory and experiments and discuss the applicability of the model to other magnetically heterogeneous systems.

II. EXPERIMENTAL RESULTS

The inverted hysteresis loops have been studied in samples of three different magnetic heterogeneous systems: amorphous YCo_2/YCo_2 bilayers, polycrystalline $Fe_{10}Ni_{90}/Fe_{10}Ni_{90}$ bilayers, and, for comparison, amorphous CoNbZr single layers annealed under an applied magnetic field.

The bilayers have been prepared on corning glass substrates by cosputtering of pure material targets.[30] Typical sputtering pressure is 10^{-3} mbar, with a base pressure in the 10^{-9} mbar range, and the thickness of each individual layer has been varied in the 10–100 nm interval. Due to the geometry of the system, the sputtering incidence direction forms an angle with the substrate normal. It allows fabrication of the magnetic layers with in-plane uniaxial anisotropy, in which the magnetic easy axis is perpendicular to the plane defined by the sputtered atomic beams. In this way, the anisotropy fields of the single layers can be as high as 100 Oe in the $Fe_{10}Ni_{90}$ layers and 200 Oe in the YCo_2 ones.[31] Then, bilayers with orthogonal individual uniaxial anisotropies are obtained by depositing a single layer, rotating 90° the sample, and, finally, growing a new magnetic layer on top.

On the other hand, magnetically heterogeneous CoNbZr single films, 0.44 μm thick, were deposited by sputtering onto continuously transported Mylar substrates. The stray field of the planar magnetron induces an in-plane uniaxial anisotropy along the transport direction. The anisotropy fields of the as-grown samples are about 30 Oe. Afterwards, the samples are annealed at 200 °C under a transverse field, applied in the perpendicular direction to the as-grown uniaxial anisotropy.[32] It favors the coexistence in the samples of different regions with orthogonal uniaxial anisotropies.

In general, we have analyzed the magnetic properties of the samples by the magneto-optical transverse Kerr effect.[33]

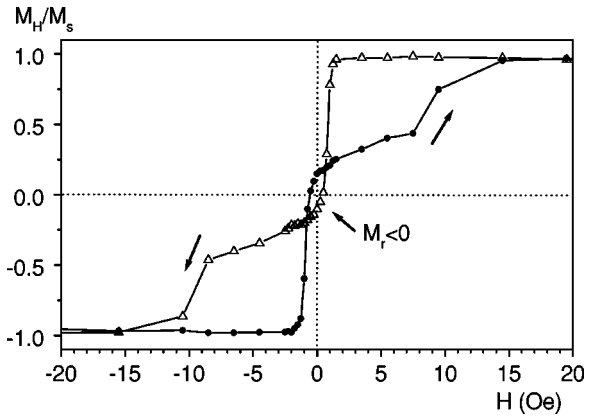

FIG. 1. Inverted hysteresis loop obtained by the magneto-optical transverse Kerr effect in a YCo_2/YCo_2 amorphous bilayer. The in-plane uniaxial anisotropies of the individual layers are orthogonal. The magnetic field is applied in the sample plane, and the sense of the field sweep is indicated by arrows.

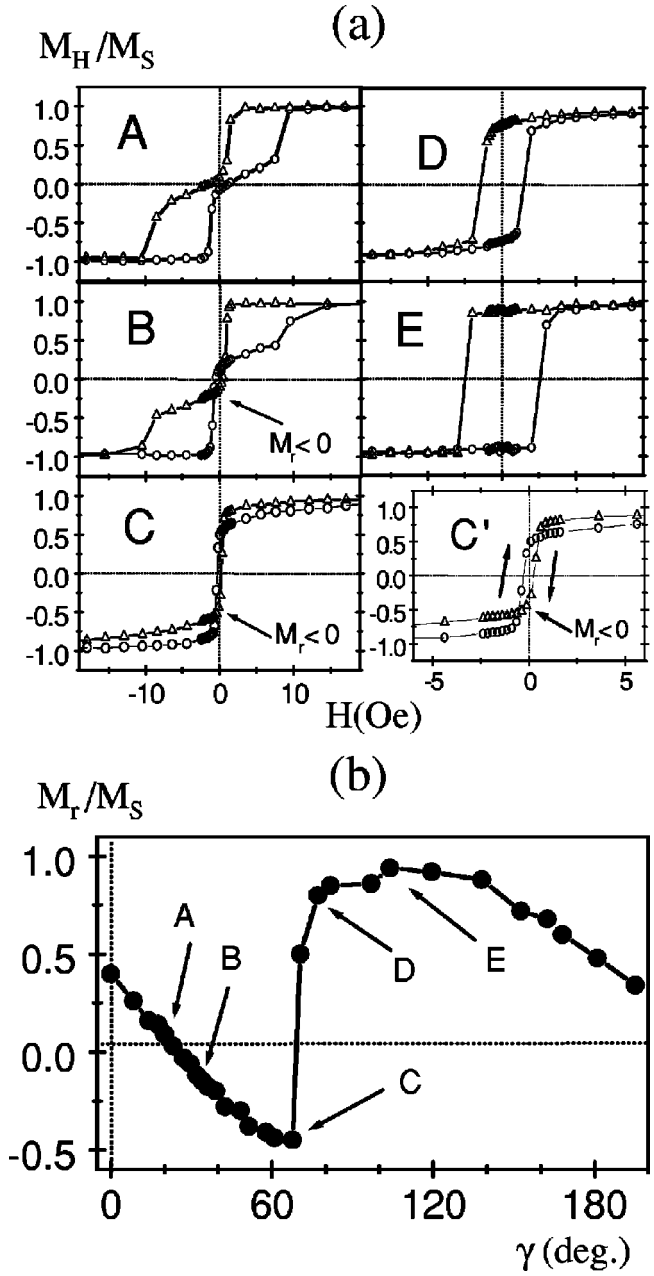

FIG. 2. (a) Kerr hysteresis loops of a YCo_2/YCo_2 (80 nm/40 nm) bilayer with orthogonal individual uniaxial anisotropies for several directions (A–E) of the applied magnetic field. As indicated in (b), they correspond to different values of the in-plane angle γ formed by the magnetic field and one of the individual easy axes. Case C′ is an enlarged view of loop C. (b) Reduced remanent magnetization (M_r/M_s) vs γ for the same sample.

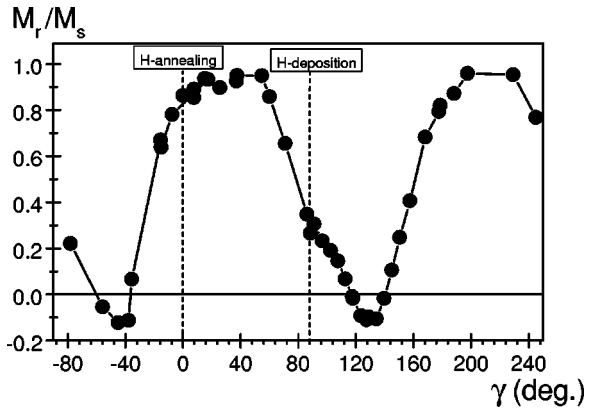

FIG. 3. Variation of the reduced remanence with the direction of the in-plane applied magnetic field in an amorphous CoNbZr film. These samples have been magnetically annealed in a transverse field. The directions of the magnetic fields applied in the growth and the annealing are indicated.

The study reveals the interesting behavior of these magnetic heterogeneous samples and, in particular, the existence of inverted hysteresis loops. Figure 1 illustrates one of these inverted loops in an amorphous YCo_2/YCo_2 bilayer. As indicated by arrows, when the magnetic field H is reduced from saturation with positive values, the magnetization sign is reversed at a positive coercive field ($H_C>0$), presenting a negative value ($M_r<0$) for $H=0$. The reciprocal dependence is measured when the field is increased from negative saturation to positive values. The analysis of the angular dependence with H shows that these negative values of M_r are observed in a certain range of applied field directions. In Fig. 2(a) we present the Kerr hysteresis loops of a YCo_2/YCo_2 (80 nm/40 nm) bilayer with **H** applied in several directions in the sample plane, that is, for different values of the angle γ between **H** and one of the individual easy axes (cases A–E). It is apparent that, for some field directions (cases B and C), inverted hysteresis loops with negative remanence are observed. The reduced remanence ($m_r=M_r/M_s$, M_r and M_s being the magnetizations at remanence and saturation, respectively) presents clear negative values as low as $m_r=-0.45$. Moreover, as is shown in Fig. 2(b), the analysis of the angular dependence reveals that the negative m_r is actually extended over a wide angular range of about 45°.

It is worth noting that these inverted hysteresis loops of the bilayers with orthogonal uniaxial anisotropy are similar to the loops calculated by Arrot, in the framework of a coherent rotation model for the magnetization of thin films with competing uniaxial and biaxial anisotropies.[22] In fact, we will show in the next section that the bilayers can be phenomenologically described by an analogous model, where the two orthogonal uniaxial anisotropies can be interpreted as one biaxial and one uniaxial anisotropies acting simultaneously on the average magnetization of the sample.

Finally, the fact that the negative values of the remanent magnetization can be observed in magnetic systems where two orthogonal uniaxial anisotropies coexist is also confirmed by the analysis of the CoNbZr films, annealed under a transverse magnetic field. Figure 3 shows the angular dependence of the reduced remanence. In this case, the inverted hysteresis loops are observed in a 25° angular range.

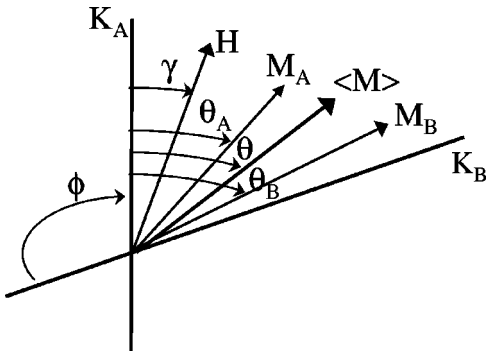

FIG. 4. Sketch with the definitions of the angles between the magnitudes involved in the total energy of the modeled bilayer.

III. THEORETICAL ANALYSIS OF HETEROGENEOUS MAGNETIC PLANAR SYSTEMS WITH COMPETITIVE UNIAXIAL ANISOTROPIES

A. Origin of the effective uniaxial and biaxial anisotropy terms

Let us consider a magnetically heterogeneous system in which two different magnetic regions coexist. These regions present uniform magnetizations M_A and M_B, uniaxial anisotropies with energy densities K_A and K_B, and their magnetic easy axes form an angle ϕ. In the case of a thin bilayer, it can be supposed that the magnetization and the anisotropies are contained in the sample plane. In our model, we also consider that the exchange interaction, which favors the parallel alignment of the interacting magnetizations, is strong enough to keep the angle between both magnetizations small.

Other additional conditions for our description are sufficiently thin individual layers and a reduced enough exchange interaction in the interface. Therefore, the Bloch domain wall, which may be present along the thickness of the bilayer, will be limited to a region at the interface with a very small thickness ϵ and a linear profile. Defining A^* and A as the exchange constants at the interface and the volume, respectively, the latter conditions can be summarized as $A^*/\epsilon(AK_{A(B)})^{1/2}<1$ (see Ref. 34). For amorphous YCo_2 typical values are $A=7\times10^{-7}$ erg/cm and $K=10^4$ erg/cm^3 (see Refs. 15 and 35), so that this relation can be expressed as $A^*/\epsilon<0.1$ erg/cm^2.

Not all of these conditions are strictly present in the studied samples; for example, in the case of the bilayer measured in Fig. 2, the total thickness is 120 nm and an extended wall is expected, so that micromagnetic calculations are needed as will be described later. However, the behavior obtained from the proposed simple model is enough to phenomenologically explain the observed experiments as well as to give a clear physical description of the processes related with the inverted hysteresis loops.

According to the definitions for the angles given in Fig. 4, the total energy of our modeled bilayers can be expressed as

$$E = V_A K_A \sin^2\theta_A + V_B K_B \sin^2(\theta_B + \phi) + V_{ex}\frac{A^*}{\epsilon^2}[1 - \cos(\theta_B - \theta_A)] - \vec{H}\cdot V\langle\vec{M}\rangle, \quad (1)$$

where V_A, V_B and V_{ex} are the volumes of the individual layers and the interface of thickness ϵ, respectively. As indicated, the magnetizations in each layer, $\vec{M_A}$ and $\vec{M_B}$, as well as the average magnetization $\langle\vec{M}\rangle$ form, respectively, angles θ_A, θ_B, and θ with the easy axis of the uniaxial anisotropy corresponding to K_A. The angle between both uniaxial easy axes is ϕ. Also, in this system, $V\langle\vec{M}\rangle = V_A\vec{M_A} + V_B\vec{M_B}$, with $V \simeq V_A + V_B$. Due to their very different dependence with ϵ, the Zeeman and anisotropy terms at the interface have been neglected in Eq. (1) with respect to the exchange term of this region.

Considering the exchange interaction hypothesis proposed in our model, that is, a small value of $\theta_A - \theta_B$, we can introduce the following change of variables in the problem:

$$\theta_A = \theta - \delta\theta_A, \quad (2a)$$

$$\theta_B = \theta + \delta\theta_B, \quad (2b)$$

$$\delta\theta \equiv \delta\theta_A \simeq \frac{m_B}{m_A}\delta\theta_B, \quad (2c)$$

where $m_{A(B)} = V_{A(B)}M_{A(B)}$. In this way, with these variables, making a series expansion in powers of $\delta\theta$, and considering the lowest power terms of the anisotropy and exchange contributions, the energy can be written as

$$E = [V_A K_A \sin^2\theta + V_B K_B \sin^2(\theta+\phi)] - \delta\theta\left[V_A K_A \sin 2\theta - \frac{m_B}{m_A}V_B K_B \sin 2(\theta+\phi)\right] + \frac{(\delta\theta)^2}{2}\left(1 + \frac{m_B}{m_A}\right)^2 V_{ex}\frac{A^*}{\epsilon^2} - VH\langle M\rangle\cos(\gamma - \theta). \quad (3)$$

The canting angle $\delta\theta$ can be obtained as a function of θ from Eq. (3) by the condition $\partial E/\partial(\delta\theta) = 0$, resulting in

$$\delta\theta = \frac{V_A K_A \sin 2\theta - \frac{m_B}{m_A}V_B K_B \sin 2(\theta+\phi)}{\left(1 + \frac{m_B}{m_A}\right)^2 V_{ex}\frac{A^*}{\epsilon^2}}. \quad (4)$$

Therefore, by substituting this value for $\delta\theta$ in Eq. (3), the energy as a function of the orientation θ of the average magnetization can be expressed as

$$E = [V_A K_A \sin^2\theta + V_B K_B \sin^2(\theta+\phi)] - \frac{1}{2}\frac{\left[V_A K_A \sin 2\theta - \frac{m_B}{m_A}V_B K_B \sin 2(\theta+\phi)\right]^2}{\left(1 + \frac{m_B}{m_A}\right)^2 V_{ex}\frac{A^*}{\epsilon^2}} - VH\langle M\rangle\cos(\gamma - \theta). \quad (5)$$

The first two terms of this equation can be rewritten as two effective anisotropies acting on the average magnetization and defined by the following relations:

$$V_A K_A \sin 2\theta - \frac{m_B}{m_A}V_B K_B \sin 2(\theta+\phi) = VK_- \sin 2(\theta + \alpha_-), \quad (6a)$$

$$V_A K_A \sin 2\theta + V_B K_B \sin 2(\theta+\phi) = VK_+ \sin 2(\theta + \alpha_+). \quad (6b)$$

By integrating Eq. (6b), the next equation can be written:

$$V_A K_A \sin^2\theta + V_B K_B \sin^2(\theta+\phi) = VK_+ \sin^2(\theta + \alpha_+) + \text{const.} \quad (6c)$$

Note that the left term of Eq. (6c) is the first term of the energy in Eq. (5).

Also, from the definitions given by Eqs. (6a) and (6b), the following relations can be found:

$$(VK_+)^2 = (V_A K_A)^2 + (V_B K_B)^2 + 2V_A V_B K_A K_B \cos 2\phi, \quad (7a)$$

$$\cos 2\alpha_+ = \frac{(VK_+)^2 + (V_A K_A)^2 - (V_B K_B)^2}{2VV_A K_+ K_A}, \quad (7b)$$

$$(VK_-)^2 = (V_A K_A)^2 + \left(\frac{m_B}{m_A}V_B K_B\right)^2 - 2\frac{m_B}{m_A}V_A V_B K_A K_B \cos 2\phi, \quad (7c)$$

$$\cos 2\alpha_- = \frac{(VK_-)^2 + (V_A K_A)^2 - \left(V_B K_B \frac{m_B}{m_A}\right)^2}{2VV_A K_- K_A}. \quad (7d)$$

Finally, using expressions (6a) and (6c), Eq. (5) for the effective density of energy can be written, except for an integration constant, as

$$\varepsilon = K_+ \sin^2(\theta + \alpha_+) - \frac{VK_-^2}{2\left(1 + \frac{m_A}{m_B}\right)^2 V_{ex}\frac{A^*}{\epsilon^2}}\sin^2 2(\theta + \alpha_-) - H\langle M\rangle\cos(\gamma - \theta), \quad (8)$$

where, together with the field contribution, there are effective uniaxial and biaxial anisotropy contributions with energy densities K_{uniax} and K_{biax}, given by

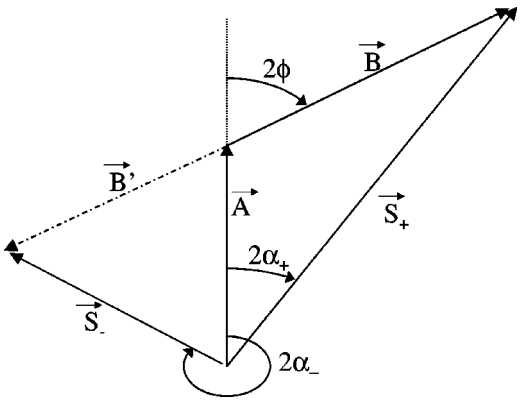

FIG. 5. Graphic method to obtain $S_{\pm}$ and $\alpha_{\pm}$.

$$K_{uniax}=K_{+}, \tag{9a}$$

$$K_{biax}=-\frac{K_{-}^{2}}{A^{*}/\epsilon^{2}}\frac{V}{V_{ex}}\frac{2}{\left(1+\frac{m_A}{m_B}\right)^{2}}. \tag{9b}$$

Equation (8) indicates that the direction of the easy axis of the resulting effective uniaxial anisotropy is given by α_{+}; also, the directions of the effective biaxial hard axes are given by α_{-}. In both cases, the easy axis of the anisotropy with K_A is taken as the reference direction. Expressions (7) generalize those proposed by Torok *et al.*,[29] as they correspond to the general case $V_A \neq V_B$ and $M_A \neq M_B$ and also allow a quantitative estimation of K_{biax} from the parameters of the system.

It is interesting to discuss some particular cases. If the two anisotropies corresponding to K_A and K_B are strictly orthogonal, with $V_A=V_B$ and $K_A=K_B$, the resulting uniaxial anisotropy will be given by $K_{uniax}=|K_A-K_B|$ and its easy axis will be parallel to the dominant anisotropy, while $K_{-}=K_A+K_B$ and the effective biaxial easy axes will be at an angle of 45° from the uniaxial one. On the other hand, in the case with $K_A=K_B=K$ but where their easy axes are not strictly orthogonal [that is, $\phi=(\pi/2-\delta\phi)$], then $K_{uniax}=2\delta\phi K$, $K_{-}=2K(1-\delta\phi^2)$, and their magnetic easy axes are practically coincident at an angle of 45° from the original uniaxial directions. As we will show later, in both these limit cases (i.e., with the effective uniaxial and biaxial easy axes forming an angle with values 0° or 45°), the inverted hysteresis loops are not observable.

The reason for the $\pm$ notation of K and α in Eqs. (6) and (7), initially proposed in Ref. 29, keeps a relation with a simple graphic representation that allows us to obtain either of the values of $K_{\pm}$ as well as the $\alpha_{\pm}$ directions. It can be done by adding or subtracting anisotropy pseudovectors, according to the angular convention defined in Fig. 5. Note that, for $\theta=0°$, Eqs. (6a) and (6b) result from the projection on the vertical axis of the $\vec{A}$, $\vec{B}$, $\vec{B'}$, $\vec{S_{+}}$, and $\vec{S_{-}}$ vectors, with modules $A=V_AK_A$, $B=V_BK_B$, $B'=(m_A/m_B)V_BK_B$, $S_{+}=VK_{+}$, and $S_{-}=VK_{-}$, respectively. It is then evident that Eqs. (7) simply establish that $|\vec{S_{+}}^2|=|\vec{A}+\vec{B}|^2$, $|\vec{S_{-}}^2|=|\vec{A}+\vec{B'}|^2$ and $\cos 2\alpha_{\pm}=(\vec{S_{\pm}}\cdot\vec{A})/|\vec{S_{\pm}}||\vec{A}|$.

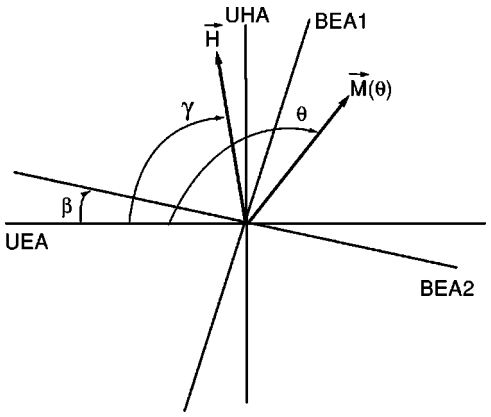

FIG. 6. Representation of the magnitudes and angles involved in Eq. (10).

B. Magnetization reversal processes by coherent rotation in magnetic systems with competitive uniaxial and biaxial anisotropies

Once we have established the origin of the effective uniaxial and biaxial anisotropies that act on the average magnetization, we are going to analyze the magnetization reversal processes in the system, considering that they are driven by coherent rotations. Although this consideration is not necessarily found in all systems where both anisotropies coexist, as in epitaxial Fe (100) thin films where the magnetization reversal is based in nucleation and domain wall movement,[36–38] we will show and discuss that the deduced behavior is in good agreement with our experimental results. It reveals that, actually, coherent rotations produce the magnetization reversal in our samples.

Using the angular definitions represented in Fig. 6, the density of energy of the system, normalized by the density of energy of the uniaxial anisotropy, can be expressed as

$$E/K_{uniax}=\sin^2(\theta)+\tfrac{1}{4}(K_{biax}/K_{uniax})\times\sin^2 2(\theta-\beta)-2h\cos(\theta-\gamma), \tag{10}$$

where $h=H/H_{K_{uniax}}=HM_s/2K_{uniax}$, β is the angle between the uniaxial and biaxial easy axes (UEA and BEA, respectively), γ is the angle between UEA and the applied magnetic field, and θ is the angle between the UEA and the magnetization. The equilibrium position of the magnetization, given by the angle θ, will be obtained by minimizing the Eq. (10) for each value of **H**. Due to symmetry considerations, the analysis can be restricted to the range $0°<\beta<45°$. To proceed with the calculation, we initially consider values of H high enough to saturate the magnetization in a certain direction; then the field is slowly decreased to determine the consecutive equilibrium positions of the magnetization. These calculations have been performed with standard routines.[39]

First, we will discuss qualitatively the magnetization rotation processes that produce the observation of inverted hysteresis loops with $m_r<0$. In particular, they will appear when the magnetic field is applied in an angular range close to the uniaxial hard axis (UHA).

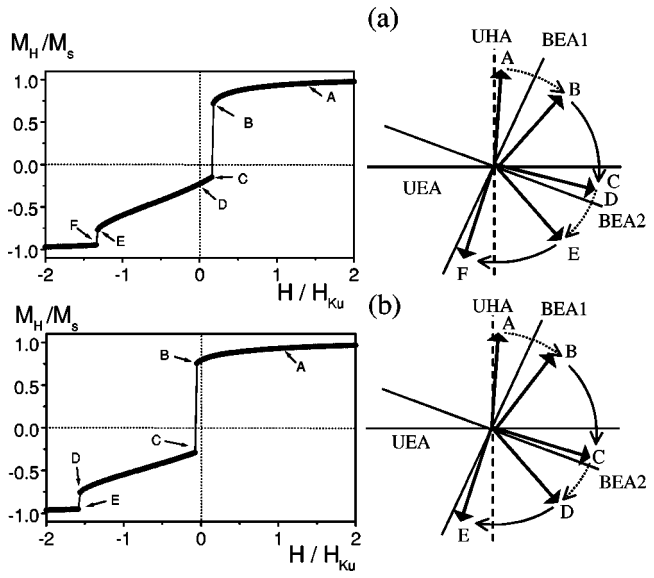

FIG. 7. Magnetization reversal processes for field applied along the UHA with $\beta=\pi/8$. (a) $K_{biax}/K_{uniax}=1.5$ $(m_r<0)$, (b) $K_{biax}/K_{uniax}=2.2$ $(m_r>0)$. Left side: calculated magnetization curves from positive to negative saturations. Right side: diagrams with the rotation processes. Note the intermediate positions of the magnetization.

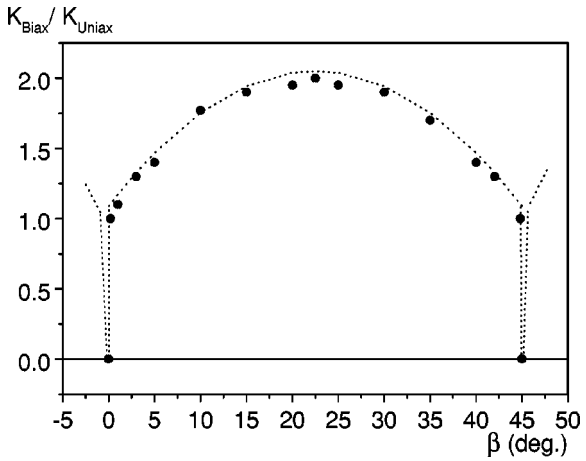

FIG. 8. Calculated $(K_{biax}/K_{uniax},\beta)$ phase diagram for the observation of inverted hysteresis loops. The dotted line is a guide to the eye. The $m_r<0$ region corresponds to that below the dotted line.

Figure 7 shows two different hysteresis loops with H parallel to the UHA, calculated for $K_{biax}/K_{uniax}=1.5$ [Fig. 7(a)] and $K_{biax}/K_{uniax}=2.2$ [Fig. 7(b)]. The sketches with the detailed magnetization rotation processes in each case are also presented. In both cases the angle between the uniaxial and biaxial easy directions is $\beta=\pi/8$.

It is interesting to carefully examine the $K_{biax}/K_{uniax}=1.5$ case, where a negative magnetization at the remanence is obtained. In this case, initially, H is at its maximum value and the magnetization is parallel to the UHA [position A in Fig. 7(a)]. As the field is reduced, the biaxial easy axis that is nearest to **M** selects the sign of the rotation, so that the magnetization continuously rotates towards the position B while $H>H_{tr1}$. At this field, H_{tr1}, **M** changes abruptly to the position C between the uniaxial and biaxial easy axes; by further decreasing the field down to $H=0$, **M** rotates continuously towards position D. In this process, from the saturation to the remanence, the total rotation of the magnetization is larger than 90°, so that $m_r<0$. As the field is increased with the opposite sign, **M** rotates continuously up to $H=H_{tr2}$ (position E), where, again, it rotates abruptly to position F. For higher field values, the magnetization moves towards the saturation.

On the other hand, in the $K_{biax}/K_{uniax}=2.2$ case, the biaxial anisotropy is strong enough to induce an equilibrium position of **M** at zero field with positive m_r value [see Fig. 7(b)].

The behavior at the remanence when the field is applied parallel to the uniaxial hard axis can be summarized as follows. If the biaxial anisotropy is not very large, the magnetization rotates from the hard axis to the easy axis in a similar way to the single uniaxial case. In this case, biaxial anisotropy plays two roles; first, the biaxial easy axis that is nearest to the applied field direction selects the rotation sign, and, second, the biaxial easy axis that is nearest to the uniaxial easy axis makes it such that the equilibrium position at the remanence is not the easy axis itself, but it is an intermediate position between both axes, so that the rotation exceeds 90° and therefore the remanent magnetization is negative. In an opposite way, if the biaxial anisotropy is strong enough, **M** rotates from the uniaxial hard axis to the nearest biaxial easy axis, and the presence of uniaxial anisotropy only produces the equilibrium position at the remanence being slightly moved towards the uniaxial easy axis.

Figure 8 shows a general vision of the ranges of K_{biax}/K_{uniax} and β values that produce inverted hysteresis loops for certain orientations of the applied magnetic field. In this graph, we present the corresponding phase diagram obtained from the systematic calculation of the hysteresis loops. Again, due to symmetry considerations, only the interval $0<\beta<\pi/4$ is analyzed. The region below the plotted curve with parabolic shape corresponds to the values of K_{biax}/K_{uniax} and β where negative remnant magnetization can be observed. It is worthwhile to note that it is not possible to find loops with $m_r<0$ for $K_{biax}/K_{uniax}>2$. The $\beta=0$ and $\beta=\pi/4$ cases correspond to singular points where inverted hysteresis loops are not observable either. On the other hand, as will be discussed later, slight deviations from these particular β values are enough to allow the presence of $m_r<0$ values (always with $K_{biax}/K_{uniax}\simeq 1.0$).

Also, note that our model predicts the existence of inverted loops for nonzero values, arbitrarily small, of K_{biax}/K_{uniax}. However, both the angular range of orientations where $m_r<0$ is observable and the modulus $|m_r|$ decrease as K_{biax}/K_{uniax} is reduced, and, also, inverted loops are present when the applied field is near to the UHA. Then, it can be expected that in real samples, for small values of K_{biax}/K_{uniax}, the magnetization processes along these **H** directions are governed by magnetization ripple (i.e., hard axis fallback[40,41]). It would result in the creation of magnetic domains and, therefore, in positive values of m_r.

For the conditions of K_{biax}/K_{uniax} and β that produce

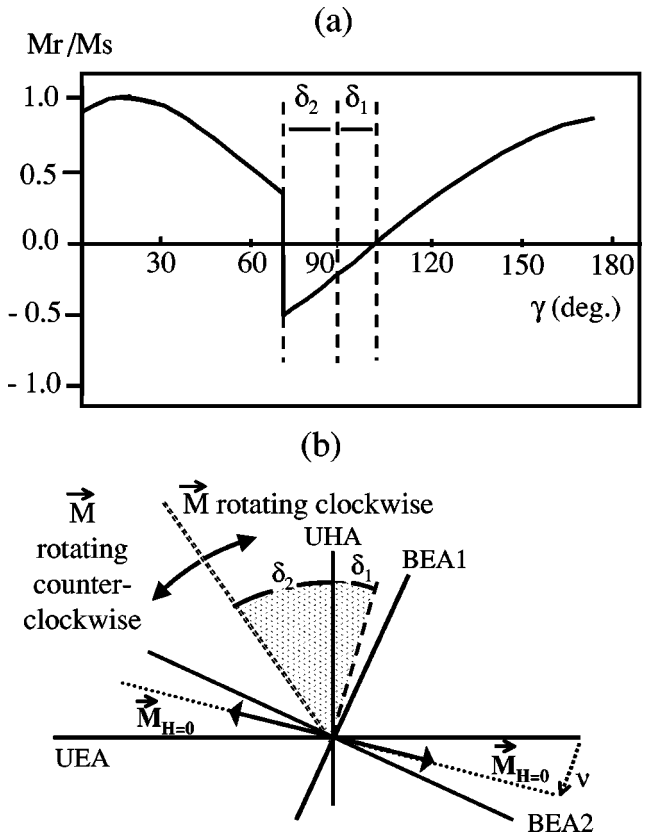

FIG. 9. (a) Sketch of the M_r/M_s vs γ curve of the meaning of the angular intervals δ_1 and δ_2. (b) Representation of δ_1 and δ_2 intervals in the magnetization rotation plane.

inverted hysteresis loops, the typical behavior of m_r as a function γ (the angle between the uniaxial easy axis and the ***H*** field) is sketched in Fig. 9(a). Negative remanence appears when the magnetic field is applied in an angular interval δ around the UHA (i.e., $\gamma=90°$), although this interval is not symmetric respect to the UHA, so that $\delta_1 \neq \delta_2$ (see Fig. 9). Besides, the most negative value of the remnant magnetization appears at the edge of a discontinuity in the m_r vs γ curve.

It is possible to give an intuitive image of the physical meanings of δ_1 and δ_2. The former, δ_1, is the angle ν between the UEA and the equilibrium direction of the magnetization at zero field ($\mathbf{M}_{H=0}$), as is easy to see in Fig. 9(b). If **H** is applied at angles higher than ν respect to the UHA, the net rotation of the magnetization will be smaller than 90° and, therefore, $m_r>0$. In this way, it is evident that the maximum value of m_r (that is, $m_r=1$ for **H** parallel to $\mathbf{M}_{H=0}$) will be found at 90° from the limit of the interval δ_1 where $m_r=0$ [see Fig. 9(a)]. On the other hand, the interval δ_2, where the remanence is also negative, is a consequence of the biaxial anisotropy, which induces the same direction in the rotation of the magnetization than in the interval δ_1 [clockwise in the sketch of Fig. 9(b)]. In particular, the amplitude of δ_2 depends in a nontrivial way on the torques exerted on the magnetization by the uniaxial anisotropy, the biaxial one, and the applied field. It produces a sharp jump in the m_r vs γ curves at the angle where m_r presents its most

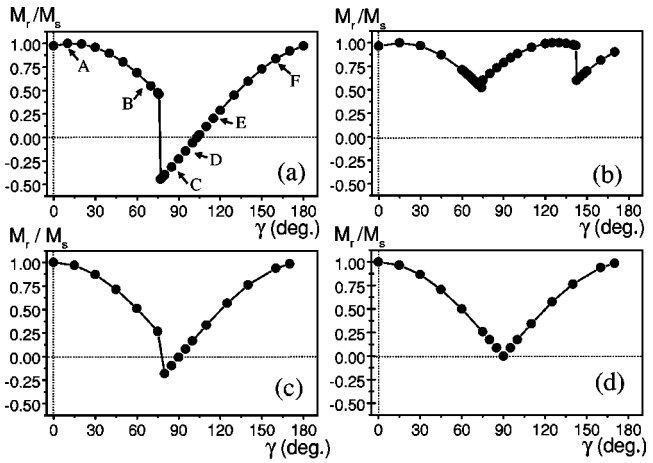

FIG. 10. M_r/M_s vs γ curves calculated for different values of K_{biax}/K_{uniax} and β. (a) $K_{biax}/K_{uniax}=1.5$, $\beta=\pi/8$; (b) $K_{biax}/K_{uniax}=2.2$, $\beta=\pi/8$; (c) $K_{biax}/K_{uniax}=1$, $\beta=1°$; (d) $K_{biax}/K_{uniax}=1$, $\beta=0$.

negative value, as at this point the net rotation of the magnetization reaches its maximum value (i.e., $90°+\delta_1+\delta_2$).

In Fig. 10 we show some particular examples, which correspond to representative behaviors of m_r vs γ curves, for different values of K_{biax}/K_{uniax} and β. Figures 10(a) and 10(b) are, respectively, the cases with $K_{biax}/K_{uniax}=1.5$ and 2.2, with a constant $\beta=\pi/8$; that is, they correspond to the loops plotted in Fig. 7. To compare both graphs, note that γ is the clockwise angle between the uniaxial easy axis and **H** direction. Again, inverted hysteresis loops only appear for $K_{biax}/K_{uniax}=1.5$. On the other hand, a biaxial-like dependence (with a quasiperiodicity of 90°) is observed for $K_{biax}/K_{uniax}=2.2$. The different dependence of δ_1 and δ_2 on the parameters can be compared in Figs. 10(a) and 10(c); in the latter, $K_{biax}/K_{uniax}=1.0$ and $\beta=1°$. Two facts are relevant: First, the lowest value of δ_1 corresponds to the smallest β, in agreement with the earlier consideration $\delta_1=\nu<\beta$. Second, the interval δ_2 does not have a direct relation with the angle β and, in particular, it can be much larger. This is consistent with the physical interpretation about the origin δ_2, related to the equilibrium condition between the torques exerted by the anisotropies and the magnetic field.

Also, the comparison of Figs. 10(c) and 10(d) reveals the influence of β on the existence of inverted hysteresis loops. In both curves, the anisotropies have been kept constant at $K_{biax}/K_{uniax}=1.0$, while the angle β has been varied. For $\beta=0$ the observed behavior [Fig. 10(d)] is similar to a pure uniaxial case; however, as proposed earlier when we presented the phase diagram, a slight change to $\beta=1°$ is enough to produce regions with negative remanence.

It is also interesting to analyze particular shapes of the hysteresis loops. Their evolution as a function of the angle γ is asymmetric around $\gamma=90°$, as can be observed in Fig. 11, where several loops corresponding to different γ values are shown for the parameters $K_{biax}/K_{uniax}=1.5$ and $\beta=\pi/8$ [cases A–F indicated in Fig. 10(a)]. For $\gamma=\nu=\delta_1$ (loop A), that is, with **H** parallel to $\mathbf{M}_{H=0}$, the loop is very similar to those obtained in a simple uniaxial sample with the field

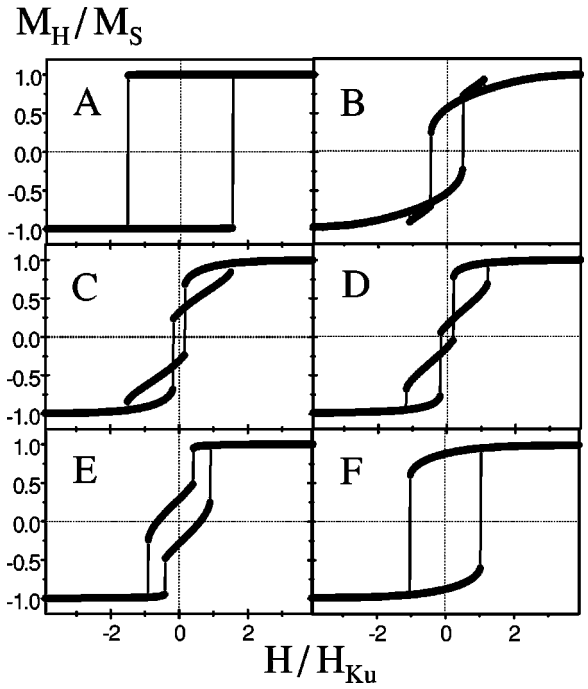

FIG. 11. Hysteresis loops calculated for $K_{biax}/K_{uniax}=1.5$ and $\beta=\pi/8$. The A–F notation corresponds to the applied field directions (γ values) indicated in Fig. 10(a).

applied along its easy axis and, therefore, $m_r=1$. As γ is increased, the loops evolve towards lower values in the remanence and the coercive field (case B) up to $\gamma=90°-\delta_2$. Over this value, the inverted hysteresis loops are observed (loops C and D) until γ reaches the value $\delta_1+\delta_2$ (where $m_r=0$). By further increasing γ and over a certain angular range, the loops present a sharp jump in the magnetization before the field has been reduced to its zero value, but they have $m_r>0$. The amplitude of the jump decreases as γ increases and, finally, a square-shaped loop is obtained for $\gamma=180°+\nu=180°+\delta_1$.

Note the qualitative good agreement between the theoretically deduced loops (Fig. 11) and the experimental magnetic behavior found in the YCo_2/YCo_2 bilayers [Fig. 2(a)]; both the peculiar shape of the loops and the evolution with the applied field direction are very similar.

C. Micromagnetic calculation for real samples

As we have shown, the proposed model is able to give a good qualitative description of the existence and behavior of inverted hysteresis loops in bilayers made of two individual uniaxial layers. On the other hand, some of the restrictions considered to construct the analytical model do not allow an accurate quantitative approximation to the results measured in real samples. For example, it is not expected that in YCo_2/YCo_2 bilayers the domain wall is collapsed in a negligible thickness. In these samples, the direct exchange interaction ($A\approx 6\times10^{-7}$ erg/cm) in amorphous YCo,[10] together with the bilayer total thickness that is larger than 100 nm, can easily produce a Bloch wall extended along an important fraction of the thickness. Also, as most of the measurements

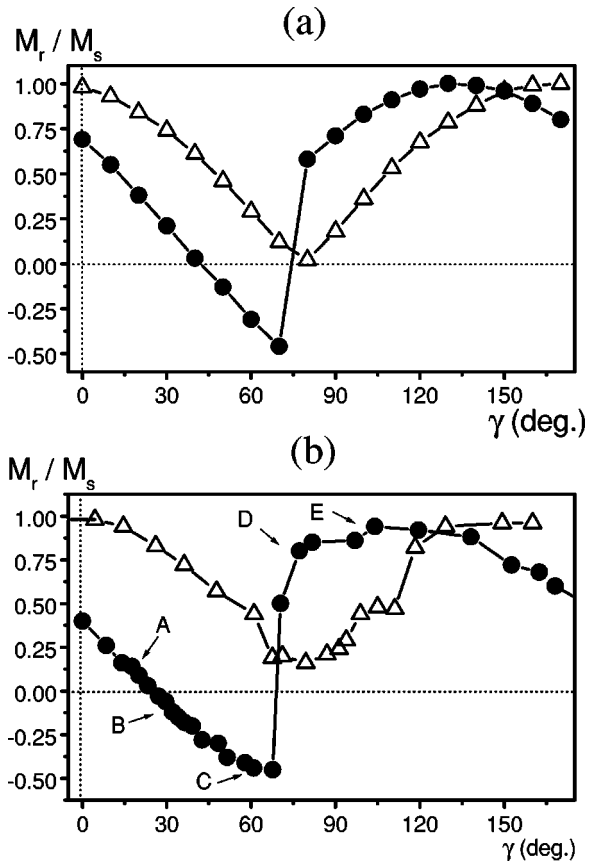

FIG. 12. (a) Micromagnetic calculation of the M_r/M_s vs γ curves predicted for the Kerr effect signal at both sides of an amorphous YCo_2/YCo_2 (80 nm/40 nm) bilayer. $A=6\times10^{-7}$ erg/cm and $K_A=K_B=10^4$ erg/cm^3 have been considered; solid circles, signal for top side (80 nm layer side); open triangles, signal for bottom side (40 nm layer side). (b) Experimental results of the M_r/M_s vs γ curves obtained by the magneto-optical transverse Kerr effect in an amorphous YCo_2/YCo_2 (80 nm/40 nm) bilayer. The meaning of the symbols is the same as in (a).

are performed by the transverse Kerr effect, it must be considered that the probe depth of this technique is typically 40 nm in this kind of amorphous materials.[42,43]

For these reasons, we have also performed a micromagnetic analysis of the behavior of bilayers that can be applied to real YCo_2/YCo_2 samples. Our calculation method evaluates the consecutive equilibrium states by decreasing the magnetic field from an initial state with a saturated magnetization; in particular, in our analysis the profile of the domain wall of the bilayers has been approximated by a hyperbolic tangent dependence.

IV. DISCUSSION

Figure 12(a) shows the results of the m_r vs γ curves obtained by micromagnetic calculations for a real sample. In this case, it corresponds to a (80 nm/40 nm) YCo_2/YCo_2 bilayer, using as parameters $A=6\times10^{-7}$ erg/cm and $K_1=K_2=10^4$ erg/cm^3, which have been previously obtained by experiments[10] in this kind of samples. Note that the predictions corresponding to the measurements by the trans-

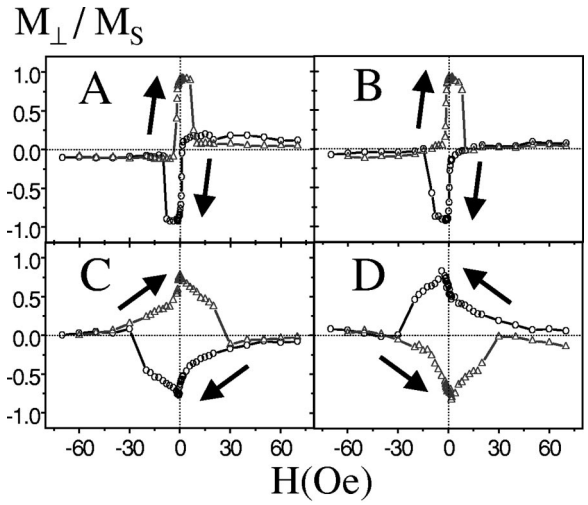

FIG. 13. $M_\perp$ vs H hysteresis loops obtained in a YCo_2/YCo_2 (80 nm/40 nm) bilayer. They correspond to the applied field orientations (A, B, C, and D) indicated in Fig. 12(b). The arrows indicate the sense of the field sweep.

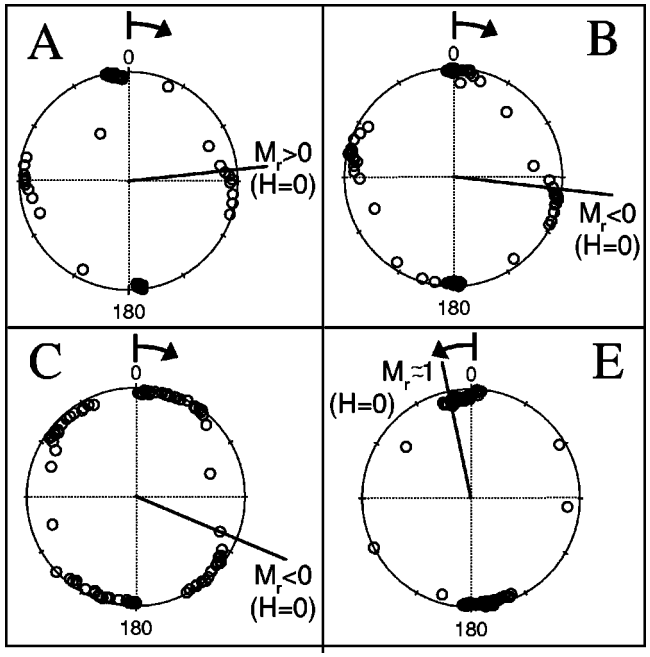

FIG. 14. Polar representation of the magnetization processes in a YCo_2/YCo_2 (80 nm/40 nm) bilayer, obtained from the $M_\parallel$ and $M_\perp$ vs H experimental loops [field directions A, B, C, and E indicated in Fig. 12(b)]. The magnetizations for $H=0$ and the rotation sense from the saturation are indicated. Note that the cases B and C correspond to $m_r<0$ and cases A and E to $m_r>0$.

verse Kerr effect at both sides of the sample are plotted. To obtain these results, an average of the magnetization projection has been performed up to a thickness of 40 nm. The behavior deduced by micromagnetic calculations is very similar to that obtained by the simple model of competing uniaxial and biaxial anisotropies with coherent rotation processes. However, some interesting details must be pointed out. First, the interval δ, where hysteresis loops with negative remanence are observed, is larger with the micromagnetic approach than the one based on the consideration of a domain wall collapsed into a negligible thickness. Also, δ can be very different at the two sides of the bilayer, both theoretically and experimentally. In the case of Fig. 12(a), it is even zero at the substrate side. Actually, this behavior could be expected from a simple analysis of the rotation processes of the average magnetization sketched in Fig. 9(b); as soon as the existence of a domain wall and the depth limit of the Kerr effect are considered, it is clear that, at one side of the bilayer, the magnetization will rotate from saturation to the remanence a larger angle than the average magnetization, resulting in more negative values of the partial m_r, while, at the other side, this angle will be lower and m_r will present either positive or less negative values.

The micromagnetic results for the YCo_2/YCo_2 bilayer [Fig. 12(a)] are in good agreement with the experimental transverse Kerr effect measurements [Fig. 12(b)]. In this case, from comparison of the experimental m_r vs γ curves at both bilayer sides, it can be estimated that the angle of the wall is about 53°. The wall profile obtained by micromagnetic calculations for this sample implies an effective wall thickness of 65 nm with an associated angle of about 45°. It is worth noting that the existence of the wall in the bilayers favors magnetization rotation processes against domain nucleations and wall movements. To clarify this, in Fig. 13 we present the experimental results of the magnetization projection ($M_\perp$) along the in-plane direction perpendicular to the applied magnetic field. These results reveal that, actually, magnetization reversal takes place by rotation processes. They correspond to four (A–D) directions of **H**, indicated in one of the m_r vs γ curves of Fig. 12(b).

Directions A and B are approximately at symmetrical γ values with respect to $m_r=0$; one direction (A) has a positive m_r, while the other (B) presents a negative remanence. Also directions C and D are symmetrical with respect to $\gamma=70°$, that is, the direction where a sharp jump in $m_r(\gamma)$ is observed and the sign of the remanence is reversed.

Two main conclusions about the magnetization rotation processes can be extracted from these experimental results. First, the experiments are consistent with our model for the sign of the rotation of the magnetization [see Fig. 9(a)]. In this way, $M_\perp$ presents opposite sign values and, therefore, different rotation directions at both sides of the sharp jump in $m_r(\gamma)$ around $m_r=0$ (δ_2 edge), either increasing the field from negative to positive values or decreasing it in the reciprocal way. On the other hand, the sign of $M_\perp$ is constant close to the other field direction where $m_r=0$ (δ_1 edge), indicating that, in this case, the rotation sign is not changed. Second, for the **H** directions in or near the region with $m_r<0$, an intermediate equilibrium position for the magnetization is observed at a direction closely perpendicular to the saturation direction. This is consistent with a model of competitive biaxial and uniaxial anisotropies. To visualize this fact, polar representations of the magnetization as the field is varied, deduced from projections parallel and perpendicular to the field ($M_\parallel$ and $M_\perp$, respectively), are plotted in Fig. 14 for different **H** directions [cases A, B, C, and E indicated in Fig. 12(b)]. Note in the polar plots A, B, and C the presence

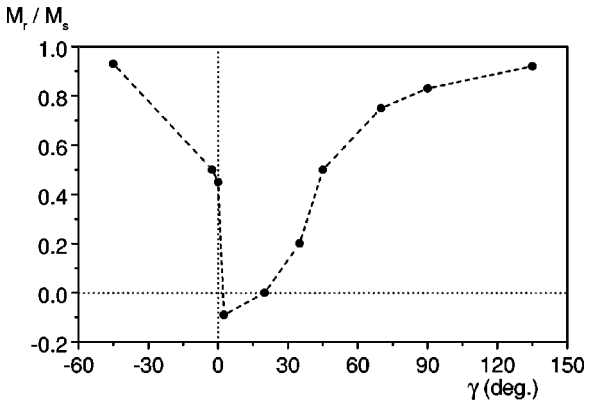

FIG. 15. m_r vs γ curve of a polycrystalline NiFe/NiFe (40 nm/40 nm) bilayer obtained by alternating gradient magnetometry. $\gamma=0°$ corresponds to the easy axis of the top NiFe layer.

of the intermediate equilibrium positions (experimental points are grouped near 90° projections) and the existence of regions with continuous rotation of the magnetization, preceded and/or followed by sharp jumps, in agreement with a model of rotation processes. In direction E, although it corresponds to the maximum value of the remanence ($m_r \approx 1$), the magnetization reversal is also driven by rotations.

As shown in Fig. 12, the extended domain wall produces $m_r(\gamma)$ curves very different at both sides of the YCo_2/YCo_2 bilayer: one with inverted hysteresis loops in a large angular range and the other with an uniaxial-like behavior. The average of both dependences, corresponding to the average magnetization of the bilayer, will result in an interval δ of **H** directions with $m_r<0$ clearly reduced with respect to that obtained in one of the sides. In fact, this reduced δ value is also in better agreement with our phenomenological model of competitive anisotropies acting on the average magnetization, as the $\delta \simeq 45°$ value experimentally observed by the Kerr effect on one side is too large to be obtained in the model for the whole sample.

To analyze the average magnetization of the bilayers, we have also performed hysteresis loops by alternating gradient magnetometry (AGM). The results of the remanence in a (40 nm/40 nm) NiFe/NiFe polycrystalline bilayer are shown in Fig. 15. Although there are problems with the precision of the applied field direction in this kind of measurements, it is clear that the $m_r(\gamma)$ behavior is analogous to that found by the Kerr effect in YCo_2/YCo_2 bilayers, with a smaller interval δ. The experimental study of the anisotropy in these samples as the thickness of the layers is varied has also been done, and will be published elsewhere; briefly, it is interesting to mention that, as the thickness is reduced (i.e., 20 nm/20 nm or 10 nm/10 nm), the contribution of the biaxial term disappears and the bilayers present an essentially uniaxial behavior. In this case, the anisotropy constants are much smaller than the values corresponding to each individual layer. In the framework of our model, the absence of the biaxial contribution can be related to the almost nonexistence of a wall ($\theta_A - \theta_B \approx 0$) across the small thickness of the bilayer.

The good agreement between the model and the experiments in the bilayers allows the analysis of the magnetic structure in other heterogeneous systems, when they present a similar behavior in the m_r vs γ curves. In fact, the results of the CoNbZr films (see Fig. 3) indicate that, as suggested earlier,[44] in these samples there is a coexistence of different regions magnetically coupled and with their uniaxial anisotropies pointing in the directions of the applied field during the growth and the annealing processes. This coupling also results in competitive uniaxial and biaxial anisotropies. The localization of those magnetic coupled regions, that is, if they are distributed along the whole volume of the sample or if they are concentrated at the interfaces, can be determined by Kerr effect measurements at both sides of the films followed by a comparison with the model.[45]

Finally, we consider some experimental results in the literature related to the behavior of magnetic systems with competitive anisotropies arranged with different symmetries. Inverted hysteresis loops have not been observed in epitaxial films and superlattices made of Fe(001). In these samples, uniaxial and biaxial anisotropies coexist with $\beta=0°$ (Refs. 37 and 38) and $\beta=45°$ (Refs. 36 and 46); the estimated values of K_{biax}/K_{uniax} are in the range $0.55<K_{biax}/K_{uniax}<30$ and the magnetization is contained in the sample plane during the reversal process. These results are consistent with the predictions of our model, as the values $\beta=0°$ and $\beta=45°$ correspond to the limits where hysteresis loops based on coherent rotations and with $m_r<0$ are not observable, independently of the ratio K_{biax}/K_{uniax} (see the phase diagram in Fig. 8). Besides, these samples usually present magnetization reversal processes of one-jump and two-jump types that are always associated with domain nucleation and wall sweeping, and not with coherent rotations.

On the other hand, loops with $m_r<0$ have been measured in epitaxial Fe(111) films grown on Si substrates with atomic steps parallel to the [110] direction.[28] These experiments have been explained with a model of competitive twofold and sixfold anisotropies and coherent rotations, which allows the existence of an out-of-plane magnetization; in this case, the existence of other energetically favorable configurations of **M** as stripe domains[30,47] has not been considered.

Inverted hysteresis loops have also been observed in Fe layers grown in W(001) substrates with stepped surfaces along a [100] direction.[48] Unfortunately, a complete study of the loops as a function of the field direction has not been reported, but in the framework of our model, the experimental results could be explained if there is a small misalignment between the biaxial axes and the uniaxial anisotropy induced by the steps and, also, $K_{uniax}>K_{biax}$ (see Fig. 8). This condition is fulfilled when the film thickness is small,[49–52] as is the case in Ref. 48.

V. CONCLUSIONS

Summarizing, the presence of inverted hysteresis loops (with $m_r<0$) is possible in heterogeneous magnetic systems as simple as bilayers made of two individual uniaxial layers. The behavior of these samples can be explained in the framework of a model proposed here, which is based on competitive uniaxial and biaxial anisotropy contributions acting on

the average magnetization of the sample. In particular, in good agreement with the experiments, it is predicted that negative remanence can be observed in a range of applied directions close to the effective uniaxial hard axis of the bilayer. We have also obtained a phase diagram for the parameters of the effective anisotropies $(K_{biax}/K_{uniax}, \beta)$, which describe the conditions where inverted loops can be observed. The understanding of the magnetization reversal processes in our samples has been further improved by micromagnetic calculations, to consider some limitations of the phenomenological model as those related to the thickness of the domain wall. This complete analysis is suitable to study the existence of different magnetically coupled regions in the sample and, also, to tailor some peculiar behaviors adequate for applications.

ACKNOWLEDGMENTS

This work has been supported by the Spanish CICYT (Grant No. MAT99-0724).

[1] L. M. Falicov, D. T. Pierce, S. D. Bader, R. Gronsky, K. B. Hathataway, H. J. Hopster, D. N. Lambeth, S. S. P. Parkin, G. Prinz, M. Salamon, I. K. Schuller, and R. H. Victoria, J. Mater. Res. **5**, 1299 (1992).

[2] For a review, see B. Dieny, J. Magn. Magn. Mater. **136**, 335 (1994).

[3] C. Aroca, M. C. Sanchez, I. Tanarro, P. Sánchez, E. López, and M. Vázquez, Phys. Rev. B **42**, 8086 (1990).

[4] M. Rührig, R. Schäfe, A. Hubert, R. Mosler, J. A. Wolf, S. Demokritov, and P. Grünberg, Phys. Status Solidi A **125**, 635 (1991).

[5] J. Unguris, R. J. Celotta, and D. T. Pierce, Phys. Rev. Lett. **67**, 140 (1991).

[6] S. T. Purcell, W. Folkerts, M. T. Johnson, N. W. E. McGee, K. Jager, J. vaan de Stegge, W. B. Zeper, W. Hoving, and P. Grünberg, Phys. Rev. Lett. **67**, 903 (1991).

[7] U. Köbler, K. Wagner, R. Wiechers, A. Fuss, and W. Zinn, J. Magn. Magn. Mater. **103**, 236 (1992).

[8] J. C. Slonczewski, Phys. Rev. Lett. **67**, 3172 (1991).

[9] R. J. Gambino, T. S. Plaskett, and R. R. Ruf, IEEE Trans. Magn. **MAG-24**, 2557 (1988).

[10] B. Dieny, D. Givord, J. M. B. Ndjaka, and J. M. Alameda, J. Appl. Phys. **67**, 5677 (1990).

[11] B. Dieny, J. P. Gavigan, and J. P. Rebouillat, J. Phys.: Condens. Matter **2**, 159 (1990).

[12] A. Layadi, J. Magn. Magn. Mater. **192**, 353 (1999).

[13] H. Chang, IBM J. Res. Dev. **6**, 419 (1962); J. Appl. Phys. **35**, 770 (1964).

[14] L. Néel, C. R. Hebd. Seances Acad. Sci. **255**, 1676 (1962).

[15] A. Yelon, in *Physics of Thin Films*, edited by G. Haas and R. E. Tun (Academic Press, New York, 1971), Vol. 6, pp. 205–300.

[16] H. Niedoba, A. Hubert, B. Mirecki, and I. B. Puchalska, J. Magn. Magn. Mater. **96**, 125 (1991).

[17] H. Niedoba, H. O. Gupta, L. H. Heyderman, I. Tomáš, and I. B. Puchalska, IEEE Trans. Magn. **MAG-26**, 1527 (1990).

[18] J. C. Slonczewski, IEEE Trans. Magn. **MAG-24**, 2045 (1988).

[19] M. Yu and Z. Zhang, J. Magn. Magn. Mater. **195**, 514 (1999).

[20] F. Suits, IEEE Trans. Magn. **MAG-26**, 2353 (1990).

[21] R. Sbiaa, H. Le Gall, Y. Braïk, and J. M. Desvignes, IEEE Trans. Magn. **MAG-31**, 3274 (1995).

[22] A. S. Arrot, in *Nanomagnetism*, edited by A. Hernando (Kluwer, Dordrecht, 1993), p. 73.

[23] M. J. O'Shea and A. Al-Sharif, J. Appl. Phys. **75**, 6673 (1994).

[24] For a review see J. Nogués and I. K. Schuller, J. Magn. Magn. Mater. **192**, 203 (1999).

[25] C. A. dos Santos and B. Rodmacq, J. Magn. Magn. Mater. **147**, L250 (1995).

[26] X. Yan and Y. Xu, J. Magn. Magn. Mater. **79**, 6013 (1996).

[27] A. Aharoni, J. Appl. Phys. **76**, 6977 (1994).

[28] M. Cougo dos Santos, J. Geshev, J. E. Schmidt, S. R. Teixeira, and L. G. Pereira, Phys. Rev. B **61**, 1311 (2000).

[29] E. J. Torok, H. N. Oredson, and A. L. Olson, J. Appl. Phys. **35**, 3469 (1964).

[30] L. M. Alvarez-Prado, G. T. Pérez, R. Morales, F. H. Salas, and J. M. Alameda, Phys. Rev. B **56**, 3306 (1997).

[31] L. M. Álvarez-Prado, R. Morales, and J. M. Alameda, J. Alloys Compd. **323-324**, 504 (2001).

[32] Samples supplied by G. Suran (L. Néel Lab-CNRS, Grenoble) and O. Acher (CEA Le Ripault, Monts).

[33] J. M. Alameda and F. López, Phys. Status Solidi A **69**, 757 (1982).

[34] H. Zijlstra, IEEE Trans. Magn. **MAG-15**, 1246 (1979).

[35] J. M. Alameda, F. H. Salas, D. Givord, and J. M. B. Ndjaka, J. Magn. Magn. Mater. **93**, 509 (1991).

[36] C. Daboo, R. J. Hicken, D. E. P. Eley, M. Gester, S. J. Gray, A. J. R. Ives, and J. A. C. Bland, J. Appl. Phys. **75**, 5586 (1994).

[37] J. R. Childress, R. Kergoat, O. Durand, J. M. George, P. Galtier, J. Miltat, and A. Schuhl, J. Magn. Magn. Mater. **130**, 13 (1994).

[38] R. P. Cowburn, J. Gray, J. Ferré, J. A. C. Bland, and J. Miltat, J. Appl. Phys. **78**, 7210 (1995).

[39] MATHEMATICA, software developed by Wolgfram Research, Inc., 1998.

[40] E. Feldtkeller, Elektron. Rechenanl. **3**, 167 (1961).

[41] J. M. Alameda, M. C. Contreras, F. Carmona, and F. López, Phys. Status Solidi A **107**, 329 (1988).

[42] F. H. Salas, C. Dehesa, G. T. Pérez, and J. M. Alameda, J. Magn. Magn. Mater. **121**, 548 (1993).

[43] C. Dehesa-Martínez, L. M. Blanco-Gutiérrez, M. Vélez, J. Díaz, L. M. Álvarez-Prado, and J. M. Alameda, Phys. Rev. B **64**, 024417 (2001).

[44] M. Takahashi, J. Appl. Phys. **33**, 1101 (1962).

[45] S. M. Valvidares, J. I. Martín, L. M. Álvarez-Prado, D. Pain, O. Acher, G. Suran, and J. M. Alameda, J. Magn. Magn. Mater. (to be published).

[46] E. Reiger, E. Reinwald, G. Garreau, M. Ernst, M. Zölfl, F. Bensch, S. Bauer, H. Preis, and G. Bayreuther, J. Appl. Phys. **87**, 5923 (2000).

[47] S. Foss, C. Merton, R. Proksh, G. Skidmore, J. Schmidt, E. D. Dahlberg, T. Pokhil, and Y. T. Cheng, J. Magn. Magn. Mater. **190**, 60 (1998).

[48] J. Chen and J. L. Erskine, Phys. Rev. Lett. **68**, 1212 (1992).
[49] M. Dumm, M. Zölfl, R. Moosbühler, M. Brockmann, T. Schmidt, and G. Bayreuther, J. Appl. Phys. **87**, 5457 (2000).
[50] C. Daboo, R. J. Hicken, E. Gu, M. Gester, S. J. Gray, D. E. P. Eley, E. Ahmad, J. A. C. Bland, R. Ploessl, and J. N. Chapman, Phys. Rev. B **51**, 15 964 (1995).
[51] M. Brockmann, M. Zölfl, S. Miethauer, and G. Bayreuther, J. Magn. Magn. Mater. **198/199**, 384 (1999).
[52] Y. B. Xu, D. J. Freeland, M. Tselepi, and J. A. C. Bland, J. Appl. Phys. **87**, 6110 (2000).